Multigrid, defect correction and upwind schemes for the steady Navier–Stokes equations

P.W. Hemker and B. Koren
Centre for Mathematics and Computer Science,
Amsterdam, The Netherlands

1. Introduction

Several Navier–Stokes methods have been developed recently (Chakravarthy et al. 1985; Schröder and Hänel 1987; Shaw and Wesseling 1986; Thomas and Walters 1985), mainly based on existing computational methods for the Euler equations. We have followed the same approach (Koren 1988a; Koren 1988b), basing the method on the Euler code (see (Hemker and Koren 1988) for an overview). Our first objective was the efficient and accurate computation of laminar, steady, two-dimensional, compressible flows at practically relevant (i.e. high) Reynolds numbers, but (still) subsonic or low-supersonic Mach numbers. The non-isenthalpic Euler code developed earlier appeared to be a good starting point for this purpose.

The resulting method is hybrid in the sense that it can be used equally well for the steady Euler equations. An upwind finite volume technique is applied for the discretisation of the convective terms in the Navier–Stokes equations. For the diffusive terms, a central finite volume technique is applied. As a basic scheme to solve the nonlinear system of discretised equations, symmetric point Gauss-Seidel relaxation is used. Herein, one or more Newton steps are used for the collective relaxation of the four unknowns in the each finite volume. Nonlinear multigrid is applied as an acceleration technique. The process is started by nested iteration. The difficulty in inverting a higher-order accurate operator is by-passed by using defect correction as an outer iteration for the nonlinear multigrid cycling. Computational results are presented for a sub- and supersonic flat plate flow, the latter with an oblique shock wave impinging on the boundary layer. The multigrid technique appears to be efficient, and reliable results are obtained.

2. Flow model

The Navier–Stokes equations considered are

$$\frac{\partial f(q)}{\partial x} + \frac{\partial g(q)}{\partial y} - \frac{1}{Re}\{\frac{\partial r(q)}{\partial x} + \frac{\partial s(q)}{\partial y}\} = 0, \tag{2.1}$$

with $f(q)$ and $g(q)$ the convective flux vectors, Re the Reynolds number, and $r(q)$ and $s(q)$ the diffusive flux vectors. As state vector q we consider the conservative vector $q = (\rho, \rho u, \rho v, \rho e)^T$, with for the total specific energy e the perfect gas relation $e = p/(\rho(\gamma - 1)) + (u^2 + v^2)/2$. The primitive quantities used so far are: the ratio of specific heats γ, density ρ, pressure p and the velocity components u and v. The quantity γ is assumed to be constant. The convective flux vectors are defined by

$$f(q) = \begin{pmatrix} \rho u \\ \rho u^2 + p \\ \rho uv \\ \rho u(e + p/\rho) \end{pmatrix}, \quad g(q) = \begin{pmatrix} \rho v \\ \rho uv \\ \rho v^2 + p \\ \rho v(e + p/\rho) \end{pmatrix}, \tag{2.2}$$

and the diffusive flux vectors by

$$r(q) = \begin{pmatrix} 0 \\ \tau_{xx} \\ \tau_{xy} \\ \tau_{xx}u + \tau_{xy}v + \frac{\partial c^2/\partial x}{Pr(\gamma-1)} \end{pmatrix}, \quad s(q) = \begin{pmatrix} 0 \\ \tau_{xy} \\ \tau_{yy} \\ \tau_{yy}v + \tau_{xy}u + \frac{\partial c^2/\partial y}{Pr(\gamma-1)} \end{pmatrix}, \tag{2.3}$$

with Pr the Prandtl number, c the speed of sound (for a perfect gas $c = \sqrt{\gamma p/\rho}$), and with τ_{xx}, τ_{xy} and τ_{yy} the viscous stresses. Assuming the diffusion coefficients to be constant and Stokes' hypothesis to hold, the stresses are written as

$$\tau_{xx} = \frac{4}{3}\frac{\partial u}{\partial x} - \frac{2}{3}\frac{\partial v}{\partial y}, \tag{2.4}$$

$$\tau_{xy} = \frac{\partial u}{\partial y} + \frac{\partial v}{\partial x}, \tag{2.5}$$

$$\tau_{yy} = \frac{4}{3}\frac{\partial v}{\partial y} - \frac{2}{3}\frac{\partial u}{\partial x}. \tag{2.6}$$

3. Discretisation method

To still allow Euler flow ($1/Re = 0$) solutions with discontinuities , the equations are discretised in their integral form. A straightforward and simple discretisation is obtained by subdividing the integration region Ω into quadrilateral finite volumes $\Omega_{i,j}$, and requiring that the conservation laws hold for each finite volume separately:

$$\oint_{\partial\Omega_{i,j}} (f(q)n_x + g(q)n_y)ds - \frac{1}{Re}\oint_{\partial\Omega_{i,j}} (r(q)n_x + s(q)n_y)ds = 0. \qquad (3.1)$$

For the evaluation of the convective flux vectors we make use of the rotational invariance of the Navier–Stokes equations. We do not do so for the diffusive flux vectors. Given our simple central discretisation of diffusive terms, use of rotational invariance for the latter is hardly advantageous. Thus, the discretised equations become

$$\oint_{\partial\Omega_{i,j}} T^{-1}f(Tq)ds - \frac{1}{Re}\oint_{\partial\Omega_{i,j}} (r(q)n_x + s(q)n_y)ds = 0, \qquad (3.2)$$

with T the rotation matrix

$$T = \begin{pmatrix} 1 & 0 & 0 & 0 \\ 0 & n_x & n_y & 0 \\ 0 & -n_y & n_x & 0 \\ 0 & 0 & 0 & 1 \end{pmatrix}. \qquad (3.3)$$

3.1 Evaluation of convective fluxes

For convection dominated flows, our objective, a proper evaluation of the convective flux vectors is of paramount importance. Based on previous experience, for this we prefer an upwind approach. Following the Godunov principle, along each finite volume wall we assume the convective flux vector to be constant, and to be determined by a constant left and right state only.

3.1.1 Approximation of left and right state

The approximation of the left and right state determines the accuracy of the convective discretisation. First- and higher-order accurate discretisations can be made. Considering for instance the numerical flux function

$$(f(q))_{i+\frac{1}{2},j} = f(q^l_{i+\frac{1}{2},j}, q^r_{i+\frac{1}{2},j})$$

where the superscripts l and r refer to the left and right side of volume wall $\Omega_{i+\frac{1}{2},j}$ (Fig. 3.1), first-order accuracy is obtained by taking

$$q^l_{i+\frac{1}{2},j} = q_{i,j}, \qquad (3.4)$$

and

$$q^r_{i+\frac{1}{2},j} = q_{i+1,j}, \qquad (3.5)$$

Higher-order accuracy can simply be obtained with the κ-schemes as introduced by van Leer (1985):

$$q^l_{i+\frac{1}{2},j} = q_{i,j} + \frac{1+\kappa}{4}(q_{i+1,j} - q_{i,j}) + \frac{1-\kappa}{4}(q_{i,j} - q_{i-1,j}), \tag{3.6}$$

and

$$q^r_{i+\frac{1}{2},j} = q_{i+1,j} + \frac{1+\kappa}{4}(q_{i,j} - q_{i+1,j}) + \frac{1-\kappa}{4}(q_{i+1,j} - q_{i+2,j}), \tag{3.7}$$

with $\kappa \in \mathbf{R}$ ranging from $\kappa = -1$ (fully one-sided upwind) to $\kappa = 1$ (central).
In (Koren 1988a) an optimal value for κ is found by giving an error analysis, using as model equation

$$\frac{\partial u}{\partial x} + \frac{\partial u}{\partial y} - \epsilon\left(\frac{\partial^2 u}{\partial x^2} + \frac{\partial^2 u}{\partial x \partial y} + \frac{\partial^2 u}{\partial y^2}\right) = 0. \tag{3.8}$$

On a grid with constant mesh size h, a finite volume discretisation which uses the κ-approximation for the convective terms and which is second-order central for the diffusive terms, yields as modified equation

$$\begin{aligned} &\frac{\partial u}{\partial x} + \frac{\partial u}{\partial y} - \epsilon\left(\frac{\partial^2 u}{\partial x^2} + \frac{\partial^2 u}{\partial x \partial y} + \frac{\partial^2 u}{\partial y^2}\right) + \\ &+h^2\left\{\frac{\kappa - 1/3}{4}\left[\frac{\partial^3 u}{\partial x^3} + \frac{\partial^3 u}{\partial y^3}\right] - \frac{\epsilon}{12}\left[\frac{\partial^4 u}{\partial x^4} + \frac{2\partial^4 u}{\partial x^3 \partial y} + \frac{2\partial^4 u}{\partial x \partial y^3} + \frac{\partial^4 u}{\partial y^4}\right]\right\} \\ &= O(h^3). \end{aligned} \tag{3.9}$$

As optimal value for κ we take the value that gives the highest possible accuracy. From (3.9) we see that a proper diffusion- dependent κ may cancel the second-order error term, which would lead to third-order accuracy. Since convection dominated problems are our main concern, for simplicity we assume this diffusion-dependence to be negligible, which leads us to $\kappa = 1/3$.

To avoid spurious non-monotonicity, a new limiter has been constructed for the $\kappa = 1/3$ approximation (Koren 1988a). Let $q^{l(k)}_{i+\frac{1}{2},j}$ and $q^{r(k)}_{i+\frac{1}{2},j}$ be the kth component ($k = 1,2,3,4$) of $q^l_{i+\frac{1}{2},j}$ and $q^r_{i+\frac{1}{2},j}$ respectively. Then a limited left and right state can be written as

$$q^{l(k)}_{i+\frac{1}{2},j} = q^{(k)}_{i,j} + \frac{1}{2}\psi(R^{(k)}_{i,j})(q^{(k)}_{i,j} - q^{(k)}_{i-1,j}), \tag{3.10}$$

and

$$q^{r(k)}_{i+\frac{1}{2},j} = q^{(k)}_{i+1,j} + \frac{1}{2}\psi(1/R^{(k)}_{i+1,j})(q^{(k)}_{i+1,j} - q^{(k)}_{i+2,j}), \tag{3.11}$$

with $\psi(R)$ the limiter considered, and $R^{(k)}_{i,j}$ the ratio

$$R^{(k)}_{i,j} = \frac{q^{(k)}_{i+1,j} - q^{(k)}_{i,j}}{q^{(k)}_{i,j} - q^{(k)}_{i-1,j}}. \tag{3.12}$$

Using this notation, the limiter constructed for the $\kappa = 1/3$ approximation reads

$$\psi(R) = \frac{R + 2R^2}{2 - R + 2R^2}. \tag{3.13}$$

3.1.2 Solution of 1D Riemann problem

Osher's scheme (Osher and Solomon 1982) has been preferred so far for the approximate solution of the standard 1D Riemann problem thus obtained. Osher's scheme has been chosen because of: (i) its continuous differentiability, and (ii) its consistent treatment of boundary conditions. (The continuous differentiability guarantees the applicability of a Newton type solution technique, which is what we make use of.) The question arises whether it is still a good choice to use Osher's scheme when diffusion also has to be modelled. Another, more widespread upwind scheme used in Navier–Stokes codes is van Leer's flux splitting scheme (van Leer 1982; Schröder and Hänel 1987; Shaw and Wesseling 1986; Thomas and Walters 1985). Reasons for its popularity are: (i) its likewise continuous differentiability, and (ii) its simplicity. The latter property is generally believed to be in contrast with Osher's scheme. (Recent work may help to reduce this difference, see e.g. (Hemker and Spekreijse 1986). In (Koren 1988a) an error analysis is given for both schemes. The analysis is confined to the steady, 2D, isentropic Euler equations for a perfect gas with $\gamma = 1$. For a subsonic flow and a first-order accurate square finite volume discretisation, the system of modified equations has been derived for both Osher's and van Leer's scheme. For both systems we considered a subsonic shear flow (the new element) along a flat plate. As a reference Lamb's approximate solution was used. Substituting Lamb's solution into the modified equation, considering the boundary layer edge at one characteristic length downstream of the leading edge, and using $Re >> 1$, we find

$$\frac{\text{error Osher}}{\text{error van Leer}} = \begin{pmatrix} 1 \\ 5(1 - 2/\pi)MRe^{-1/2} \\ 1/2 \end{pmatrix} \tag{3.14}$$

where M is the outer flow Mach number. From (3.14) it appears that, when compared with Osher's, van Leer's scheme deteriorates for increasing Re.

3.2 Evaluation of diffusive fluxes

For the evaluation of the diffusive fluxes at a volume wall, it is necessary to computer ∇u , ∇v and ∇c^2 at the wall. For this we use a standard technique (Peyret and Taylor 1983). To compute for instance $(\nabla u)_{i+\frac{1}{2},j}$, we use Gauss' theorem:

$$(\nabla u)_{i+\frac{1}{2},j} = \frac{1}{A_{i+\frac{1}{2},j}} \oint_{\partial\Omega_{i+\frac{1}{2},j}} u\mathbf{n}ds, \tag{3.15}$$

with $\mathbf{n} = (n_x, n_y)^T$; $\partial\Omega_{i+\frac{1}{2},j}$ the boundary and $A_{i+\frac{1}{2},j}$ the area of a quadrilateral dummy volume $\Omega_{i+\frac{1}{2},j}$ (Fig. 3.2) of which the vertices $\mathbf{z} = (x, y)^T$ are defined by:

$$\mathbf{z}_{i,j\pm\frac{1}{2}} = \frac{1}{2}(\mathbf{z}_{i-\frac{1}{2},j\pm\frac{1}{2}} + \mathbf{z}_{i+\frac{1}{2},j\pm\frac{1}{2}}). \tag{3.16}$$

A similar expression exists for $\mathbf{z}_{i\pm\frac{1}{2},j}$.
The line integral $\oint_{\partial\Omega_{i+\frac{1}{2},j}} u\mathbf{n}ds$ is approximated by

$$\begin{aligned}\oint_{\partial\Omega_{i+\frac{1}{2},j}} u\mathbf{n}ds \;=\; & u_{i+1,j}(\mathbf{z}_{i+1,j+\frac{1}{2}} - \mathbf{z}_{i+1,j-\frac{1}{2}}) \\ & + u_{i+\frac{1}{2},j+\frac{1}{2}}(\mathbf{z}_{i,j+\frac{1}{2}} - \mathbf{z}_{i+1,j+\frac{1}{2}}) \\ & + u_{i,j}(\mathbf{z}_{i,j-\frac{1}{2}} - \mathbf{z}_{i,j+\frac{1}{2}}) \\ & + u_{i+\frac{1}{2},j-\frac{1}{2}}(\mathbf{z}_{i+1,j-\frac{1}{2}} - \mathbf{z}_{i,j-\frac{1}{2}}),\end{aligned} \tag{3.17}$$

with for $u_{i+\frac{1}{2},j\pm\frac{1}{2}}$ the central expression

$$u_{i+\frac{1}{2},j\pm\frac{1}{2}} = \frac{1}{4}(u_{i,j} + u_{i,j\pm1} + u_{i+1,j} + u_{i+1,j\pm1}). \tag{3.18}$$

Similar expressions are used for the other gradients and other walls. For sufficiently smooth grids this central diffusive flux computation is second-order accurate.

4. Solution method

To efficiently solve the system of discretised equations, symmetric point Gauss–Seidel relaxation, accelerated by nonlinear multigrid (FAS), is applied. With the scalar convection diffusion equation (3.8) as a model, local mode analysis shows that 'symmetric point Gauss–Seidel + multigrid' converges fast for the first-order discretised equation, for any value

of the mesh Reynolds number h/ϵ (Koren 1988b). However, it appears to converge very slowly for the higher-order ($\kappa = 1/3$)discretised equation, for small and moderately large values of h/ϵ. It even appears to diverge for large values of h/ϵ (Koren 1988b). Clearly, the cause is the higher-order discretisation of the convection operator. No cure can be found in using some other $\kappa \in [-1, 1]$. As with the Euler equations (Hemker 1986; Koren 1988c), the difficulty in inverting the higher-order operator is by-passed by introducing iterative defect correction (IDeC) as an outer iteration for the nonlinear multigrid cycling . Let $F_h(q_h)$ denote the full, higher-order accurate operator, and $\tilde{F}_h(q_h)$ the less accurate operator that can be easily inverted. Then iterative defect correction can be written as

$$\begin{aligned} &\tilde{F}_h(q_h^1) = 0, \\ &\tilde{F}_(q_h^{n+1}) = \tilde{F}_h(q_h^n) - \omega F_h(q_h^n), \quad n = 1, 2, \ldots, N. \end{aligned} \tag{4.1}$$

where n denotes the nth iterand, and ω a damping factor. (The standard value for ω is $\omega = 1$). Special attention has been paid to the choice of the approximate operator $\tilde{F}_h(q_h)$ for the Navier–Stokes equations. The operator necessarily has only first-order accurate convection, but the amount of diffusion can be chosen freely. This freedom has been exploited by analyzing three approximate operators $\tilde{F}_h$: (i) an operator with full, second-order accurate diffusion, (ii) an operator with partial diffusion, and (iii) an operator without diffusion. The *first approximate operator* most closely resembles the higher-order operator F_h, and therefore has the best convergence properties. For sufficiently smooth problems and a second-order accurate F_h, theory (Hackbusch 1985) predicts the solution to be second-order accurate after a single IDeC-cycle for the first approximate operator. Theory does not give this guarantee for the other approximate operators. The *second approximate operator* neglects the cross derivatives in the diffusive terms, but it has full second-order diffusion, stemming from the remaining derivatives. The special feature of this operator is that, for the evaluation of the convective and diffusive fluxes in the Navier–Stokes equations, the same five-point data structure can be used. The operator combines elegance and simplicity with a rather good resemblance to the higher-order operator. The *third approximate operator* considered was already known from the Euler work. Given its successful application there, it may be expected to be suitable for very large values of the mesh Reynolds number. Local mode analyses with (3.8) as a model equation, and experiments with the Navier–Stokes equations showed the first approximate operator to have the best convergence properties indeed. The faster convergence clearly compensates for its relative complexity. The results presented in the next section have all been obtained with this operator.

Though the mesh Reynolds numbers in the computations performed were

large, we obeyed the multigrid requirement (cf. (Hackbusch 1985)) $m_r + m_p > 2m$, where m_r and m_p denote the order of accuracy of the defect restriction and the correction prolongation respectively, and where $2m$ denotes the order of the differential equation(s) considered. We used a piecewise constant restriction ($m_r = 1$) and a piecewise bilinear prolongation ($m_p = 2$).

5. Numerical results

To evaluate the computational method developed, the following flow problems have been considered: (i) a subsonic flat plate flow, and (ii) a supersonic flat plate flow with oblique shock wave-boundary layer interaction. For the subsonic problem, the Blasius solution is used as a reference. For the supersonic problem comparisons are made with experimental results obtained by Hakkinen et al. (1958). For both flow problems we used: $\gamma = 1.4$ and $Pr = 0.71$.

5.1 Subsonic flat plate flow

The geometry, the boundary conditions and the coarsest grid used for this flow problem are given in Fig. 5.1. As far as convection is concerned, the eastern boundary has been considered as an outflow boundary. For diffusion the northern, southern and eastern boundary have been assumed to be far-field boundaries with zero diffusion. For this problem we only used grids composed of square finite volumes. As a coarsest grid in all multigrid computations we used the 4×2 grid given in Fig. 5.1.

5.1.1 Osher's and van Leer's scheme

To compare Osher's and van Leer's scheme, we performed for both schemes an experiment with $h-$ (mesh size) and Re variation, using the first-order approximation only (because this will best show the differences). Results obtained are given in Fig. 5.2. The results clearly show the superiority of Osher's scheme, in particular under hard conditions (first-order approximation, high mesh Reynolds number). Notice that van Leer's scheme deteriorates as predicted (compared to Osher's) for increasing Re. However, notice also that for *both* schemes the exact numerical solution (i.e. a vanishing boundary layer) has been obtained for $Re = 10^{100}$. For van Leer's scheme this could only be obtained by a careful treatment of the solid wall boundary condition for the convective part (Koren 1988a).

In the further experiments we continued with Osher's scheme only.

5.1.2 Multigrid behaviour

To investigate the convergence properties of the nonlinear multigrid technique we considered the subsonic flat plate flow at $Re = 100$, using the first-order discretised equations and Osher's approximate Riemann solver.

We are interested in the measure of grid independence of the convergence rate, the multigrid effectiveness and the influence of the order of accuracy of the prolongation. To measure the grid independence, we performed 20 FAS-cycles on a $16 \times 8-$, a $32 \times 16-$, and a 64×32 grid. For the multigrid effectiveness we performed 21 symmetric relaxation sweeps on the 64×32 grid. Further, to investigate the influence of the order of accuracy of the prolongation, we performed again 20 FAS-cycles with the 64×32 grid as finest grid, but now with the piecewise constant correction prolongation ($m_p = 1$, so violating the rule $m_r + m_p > 2m$). The results are given in Fig. 5.3. They clearly show that, for the flow considered, the multigrid method is nearly grid-independent and highly effective. The effect of the order of accuracy of the prolongation appears to be negligible.

5.1.3 Convergence to first- and second-order accuracy

Theory predicts that a single FAS-cycle may be sufficient for obtaining first-order accuracy (Hemker 1986). Further, as mentioned before, for smooth problems theory predicts a single IDeC-cycle to be sufficient for obtaining second-order accuracy (Hackbusch 1985). To investigate the convergence properties with respect to these two predictions we computed again solutions on the $16 \times 8-, 32 \times 16-$, and 64×32 grids for $Re = 100$. We performed the computations for successively the first-order and the (non-limited) $\kappa = 1/3$ approximation. Solutions obtained after 1 FAS-cycle and 1 IDeC-cycle (with inside the latter only a single FAS-cycle) are given in Fig. 5.4a and 5.4b respectively. Assuming the Blasius solution to be the exact solution, it can be verified that the results obtained (more or less) satisfy the theoretical predictions. In order to compare, for both discretisations the fully converged solutions (square markers) have been given. Additionally, as a contrast, in Fig. 5.4a, the single 64×32 grid solutions as obtained after 1,2,3 and 4 symmetric relaxation sweeps have been given (for the first-order discretisation only). The latter solutions clearly show once more the effectiveness of the multigrid technique.

5.2 Supersonic flat plate flow with oblique shock wave–boundary layer interaction

As reference test case from Hakkinen et al. (1958) we considered the experiment performed at $Re = 2.96 \times 10^5$. At first we tried to make a satisfactory grid. Since the present code has the possibility to compute Euler flows, it is easy to optimise the grid for convection only. For the present test case this led via the 80×32 grid shown in Fig. 5.5a to the 80×32 grid in Fig. 5.5b. The corresponding inviscid surface pressure distributions as obtained with the first-order, the non-limited $\kappa = 1/3$ and the limited $\kappa = 1/3$ approximation, are given in Fig. 5.6. The poor solution quality on the rectangular grid is clear. (For boundary conditions etc., we refer to

(Koren 1988b).)

Together with the measured data, the computed viscous surface pressure distributions are given in Fig. 5.7. (For convergence histories we refer to (Koren 1988b)). First we consider the results obtained on the rectangular grid. Given the bad inviscid solutions, obtained on the regular grid, it should be noticed that the good resemblance of the experimental and the second-order accurate viscous surface pressure distribution is absolutely fake. Since for this standard test case most authors use rectangular grids, and since most codes smear out discontinuities which are not aligned with the grid, a lot of good resemblance ever found for this test case might in fact be deceptive. Considering the results obtained on the oblique grid and comparing at first the computed surface pressure distributions, we see that diffusion has done its job in qualitatively different ways. In downstream direction, the second-order pressure distribution in the interaction region shows successively: a compression, a plateau and another compression. The computed second-order accurate surface pressure distribution is characteristic for a shock wave–boundary layer interaction with separation bubble (i.e. with separation and reattachment), whereas the first-order distribution typically is the distribution belonging to a non-separating flow. Given the occurrence of a separation bubble in the experimental results indeed, the first-order solution (on this 80×32 grid) has to be rejected. Comparing the second-order and measured surface pressure distribution, it appears that the latter is more strongly diffused. An explanation for this quantitative difference is lacking. Due to all kinds of uncertain influences a detailed quantitative comparison is probably impossible. Uncertain factors in the experiment are for instance: cross flow influences (3D effects), non-observed though influential turbulence, some slight heat transfer through the wall etc. Uncertain influences in the computation are for instance: a possibly too crude boundary condition treatment somewhere, the neglect of temperature dependence in the diffusion coefficients, and so on.

6. Conclusions

In this paper we showed that the geometric multigrid method (combined with iterated defect correction) is a feasible method for the efficient solution of the steady full Navier–Stokes equations.

An important practical result of the present paper is the illustrated importance of carefully checking the reliability of a computed Navier–Stokes solution. In particular, the reliability should be checked with respect to the numerical errors introduced by the discretisation of the convective part. *This seems a trivial remark, but it appears that one is not sufficiently aware of this problem in practice.* The present approach allows an easy check of false diffusion: the same code can be used for both viscous and inviscid

flow computations.

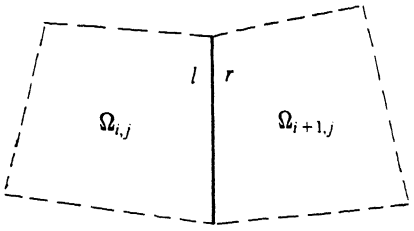

Fig. 3.1. Volume wall $\partial\Omega_{i+\frac{1}{2},j}$

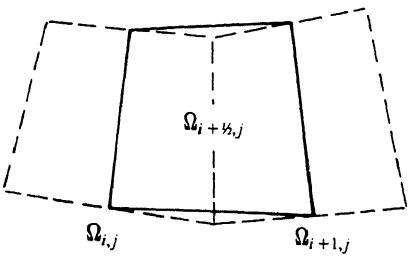

Fig. 3.2. Shifted volume $\Omega_{i+\frac{1}{2},j}$

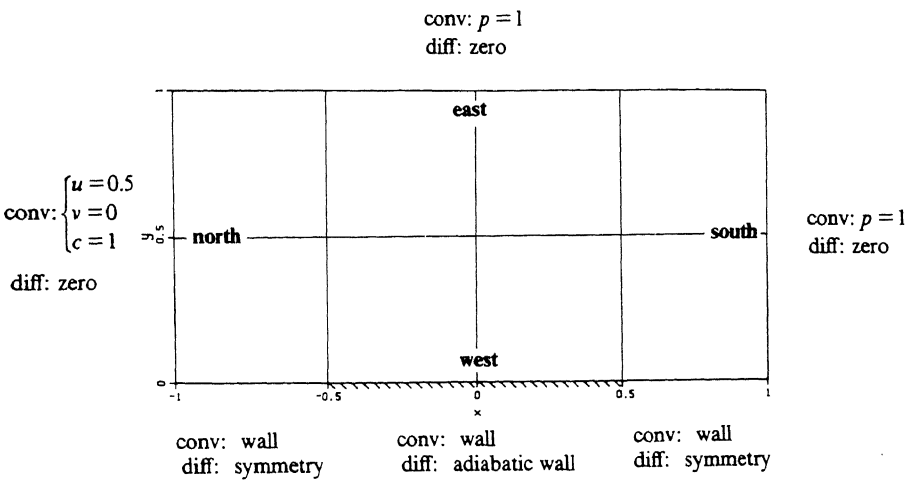

Fig. 5.1. Geometry, boundary conditions and coarsest grid subsonic flat plate flow (conv: convection, diff: diffusion)

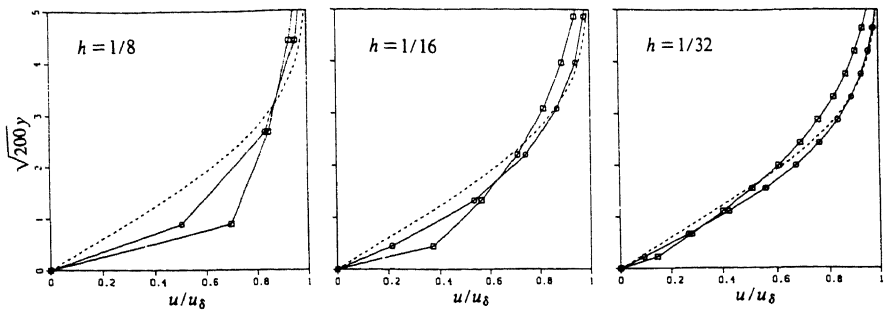

a. h−variation at $Re = 100$ (○: Osher,□: van Leer).

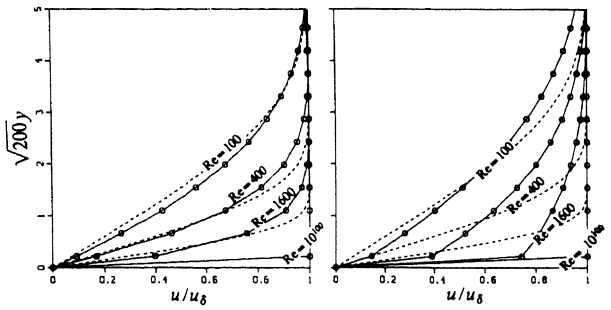

b. Re−variation at $h = 1/32$ (left: Osher, right: van Leer).

Fig. 5.2. Velocity profiles at $x = 0$ for the subsonic flat plate flow.
(——: Blasius solution)

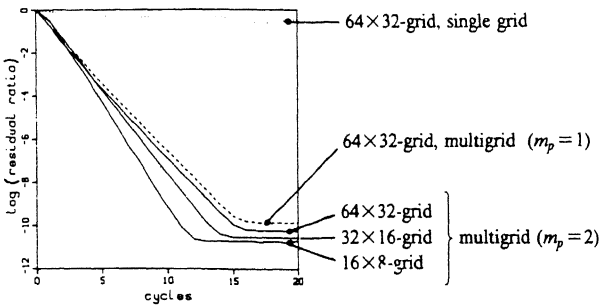

Fig. 5.3. Multigrid behaviour

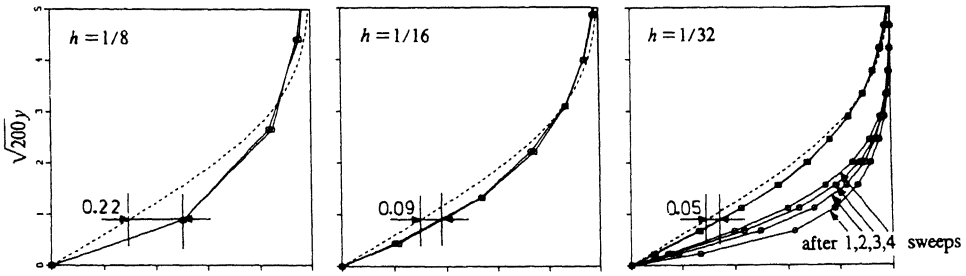

a. First-order (○: after 1 FAS-cycle, □: after 20 FAS-cycles).

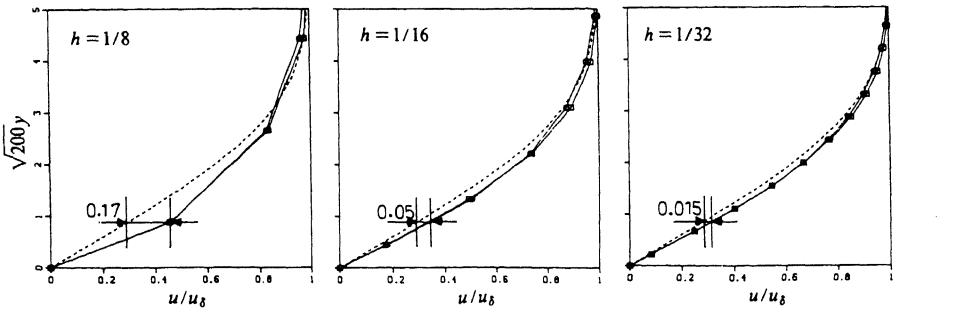

b. Non-limited second-order
(○: after 1 IDeC-cycle, □: after 50 IDeC-cycles).

Fig. 5.4. Velocity profiles at $x = 0$ for the subsonic flate flow.
(——: Blasius solution)

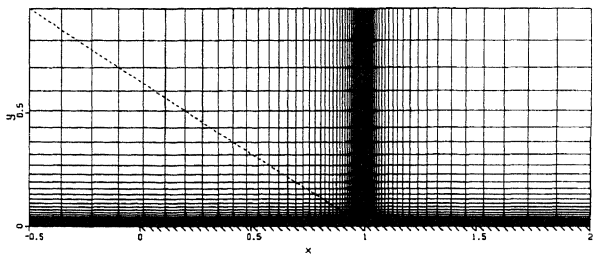

a. Rectangular grid (——: shock wave).

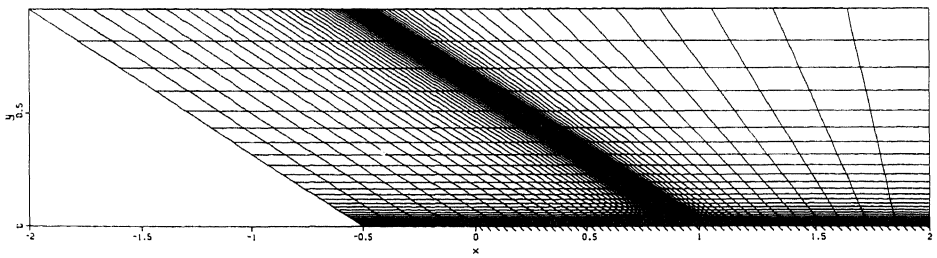

b.Oblique grid.

Fig. 5.5. Finest grids supersonic flat plate flow

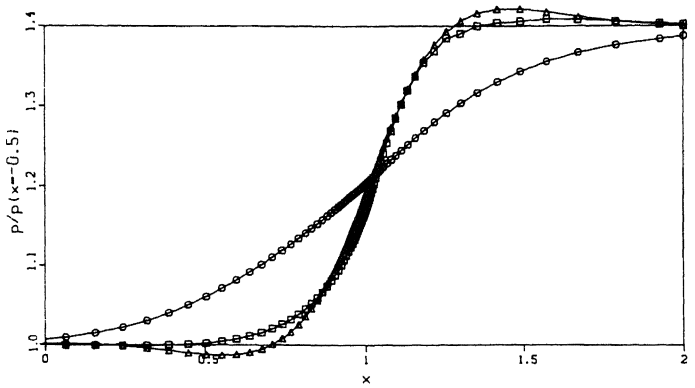

a. On rectangular grid.

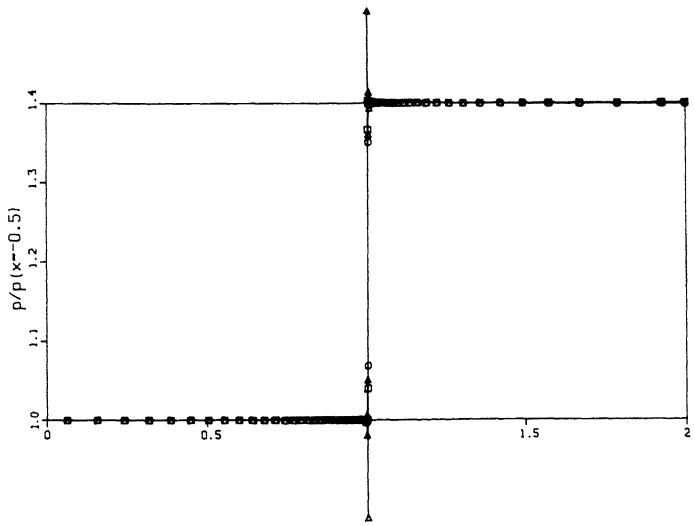

b. On oblique grid.

Fig. 5.6. Inviscid surface pressure ditributions supersonic flat plate flow
(○: first-order, △: non-limited higher-order, □: limited higher-order)

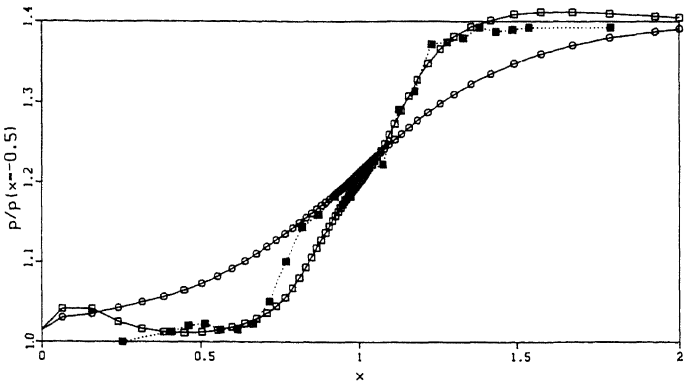

a. On rectangular grid.

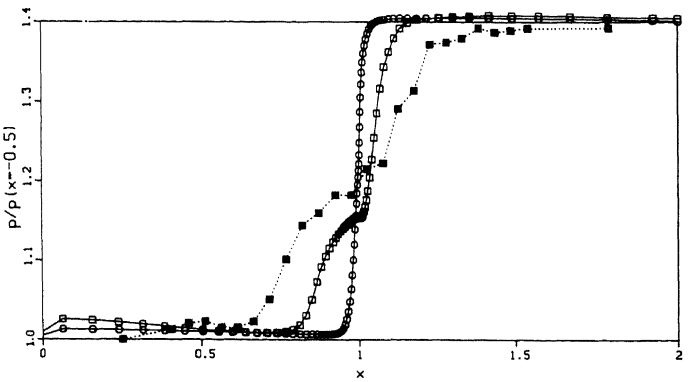

b. On oblique grid.

Fig. 5.7. Viscous surface pressure distributions supersonic flat plate flow
(○: first-order, □: limited second-order, ■ : measured)

Acknowledgement

This work was supported, in part, by the European Space Agency (ESA), via Avions Marcel Dassault–Bréguet Aviation (AMD-BA).

References

Chakravarthy, S., Szema, K., Goldberg, U., Gorski, J., and Osher, S. (1985). Application of a new class of high accuracy TVD schemes to the Navier–Stokes equations. AIAA paper 85–0165.

Hackbusch, W. (1985). *Multi-Grid Methods and Applications.* Springer, Berlin.

Hakkinen, R., Greber, I., Thrilling, L., and Abarbanel, S. (1958). The interaction of an oblique shock wave with a laminar boundary layer. NASA-memorandum 2-18-59 W.

Hemker, P. (1986). Defect correction and higher order schemes for the multigrid solution of the steady Euler equations. In *Proceedings of the Second European Conference on Multigrid Methods, Cologne 1985.* Springer, Berlin.

Hemker, P. and Koren, B. (1988). Defect correction and nonlinear multigrid for the steady Euler equations. In *Lecture Series on Computational Fluid Dynamics*, Von Karman Institute for Fluid Dynamics, Rhode–Saint–Genèse, Belgium.

Hemker, P. and Spekreijse, S. (1986). Multiple grid and Osher's scheme for the efficient solution of the steady Euler equations. *Appl. Num. Math.*, 2:475–493.

Koren, B. (1988a). Upwind schemes for the Navier–Stokes equations. In *Proceedings of the Second International Conference on Hyperbolic Problems, Aachen 1988.* Vieweg, Braunschweig.

Koren, B. (1988b). Multigrid and defect correction for the steady Navier–Stokes equations. In *Proceedings of the Fourth GAMM Seminar on Robust Multigrid Methods, Kiel 1988.* Vieweg, Braunschweig.

Koren, B. (1988c). Defect correction and multigrid for an efficient and accurate computation of airfoil flows. *Journal of Computational Physics.* (to appear in 1988).

van Leer, B. (1982). Flux–vector splitting for the Euler equations. In *Proceedings of the 8th International Conference on Numerical Methods in Fluid Dynamics, Aachen 1982.* Springer, Berlin.

van Leer, B. (1985). Upwind–difference methods for aerodynamic problems governed by the Euler equations. In *Proceedings of the 15th AMS–SIAM Summer Seminar on Applied Mathematics*, Scripps Institution of Oceanography, 1983. AMS, Providence, Rhode Island.

Osher, S. and Solomon, F. (1982). Upwind–difference schemes for hyperbolic systems of conservation laws. *Mathematics of Computation*, 38:339–374.

Peyret, R. and Taylor, T. (1983). *Computational Methods for Fluid Flow.* Springer, Berlin.

Schröder, W. and Hänel, T. (1987). An unfactored implicit scheme with multigrid acceleration for the solution of the Navier–Stokes equations. *Computers and Fluids*, 15:313–336.

Shaw, G. and Wesseling, P. (1986). Multigrid solution of the compressible Navier–Stokes equations on a vector computer. In *Proceedings of the 10th International Conference on Numerical Methods in Fluid Dynamics, Beijing 1986.* Springer, Berlin.

Thomas, J. and Walters, R. (1985). Upwind relaxation algorithms for the Navier–Stokes equations. AIAA paper 86–1501.